Journal of Control, Automation and Electrical Systems (2018) 29:541–550
https://doi.org/10.1007/s40313-018-0398-3

Design of Wide-Area Damping Controllers Incorporating Resiliency to Permanent Failure of Remote Communication Links

Murilo Eduardo Casteroba Bento[1] · **Roman Kuiava**[2] · **Rodrigo Andrade Ramos**[1]

Received: 4 April 2018 / Revised: 14 June 2018 / Accepted: 13 July 2018 / Published online: 23 July 2018

Abstract
The synchrophasor data provided by wide-area measurement systems have potential applications in electric power systems such as the use of these measurements as control inputs of wide-area damping controllers (WADCs) for small-signal stability enhancement. However, synchrophasor data are particularly vulnerable to cyber attacks (such as denial-of-service attacks) that can cause communication link failures in a smart grid communication network and, consequently, compromise the power system stability. In order to reduce the impact of communication failures on the performance of a WADC, this paper proposes a method to design a WADC considering robustness to multiple operating points, time delays in the communication channels and possible permanent loss of communication signals in the input and the output of the controller (which may be due, e.g., to denial-of-service cyber attacks). The performance of the designed controller is evaluated using modal analysis and nonlinear time-domain simulations in one of the IEEE benchmark systems to validate the results: the Simplified 14-Generator Model of the Southeastern Australian Power System.

Keywords Wide-area damping control · Communication failure · Linear matrix inequalities · Cyber security · Denial-of-service attacks

1 Introduction

The expansion of the wide-area measurement systems (WAMS) is expected to provide a number of important features in smart grids (Li et al. 2010). WAMS present phasor measurement units (PMUs) that are used to measure real-time current and voltage phasors in power network and to send the synchronized data at a specific rate to the phasor data concentrators (PDCs). The synchronization of the data of all PMUs of the grid is reached by the use of the global position system (GPS) clock (De La Ree et al. 2010; Tran and Zhang 2018).

The PMU data provide valuable information about the state of the system that can be used for a wide variety of applications such as state estimation (Ghahremani and Kamwa 2016), real-time monitoring of the system (Zhao et al. 2016), wide-area control (Surinkaew and Ngamroo 2016) and protection (Biswal et al. 2016; Ghorbani et al. 2017). Due to its importance to power system monitoring, control and protection, the manipulation of PMU data is particularly attractive avenues for cyber attackers that intend to disrupt and damage the power infrastructure (Sikdar and Chow 2011). Besides, the synchrophasor measurement data are usually transferred over public domain networks such as the Internet, thereby making them susceptible to a number of attacks. The most common communication protocol used by PMUs to transmit their data is defined in the IEEE C37.118 standards.

Cyber attacks such as denial-of-service (DoS) attacks, false data injection attacks and cyber-physical switching attacks can affect the dynamic performance of the power system. Resilience against these types of attacks must be addressed through a defense-in-depth paradigm whereby pre-

This work was financially supported by Fundação de Amparo à Pesquisa do Estado de São Paulo (FAPESP) under Grant No. 2015/24245-8.

✉ Murilo Eduardo Casteroba Bento
murilo.bento@usp.br

Roman Kuiava
kuiava@eletrica.ufpr.br

Rodrigo Andrade Ramos
rodrigo.ramos@ieee.org

[1] University of Sao Paulo, Av. Trabalhador Sao-Carlense, 400, Sao Carlos, SP 13566-590, Brazil

[2] Federal University of Parana, Rua Cel. Francisco Heraclito dos Santos, Curitiba, PR 81531-980, Brazil

vention, detection and reaction approaches for protection are employed at various levels (Farraj et al. 2018).

In DoS attacks, an adversary interrupts the operation of the cyber component of the power grid by jamming the communication channels, attacking network protocols and flooding the network traffic. Consequently, DoS attacks lead to disruptions and excessive time delays in the communication network. These disruptions and time delays cause, respectively, permanent loss of communication channels and high values on the communication rates (or packet drops) between the sensors, actuators and control systems (Farraj et al. 2018). In Liu et al. (2013), the authors showed that, under a properly designed DoS attack sequences on the communication channels, the power system can become unstable. If attacked, measurement packets sent from sensors through this channel will be lost. In this work, we focus on a strategy to enhance the resilience of the smart grid subject to cyber attacks that disrupt a communication channel of a wide-area damping controller and may compromise the small-signal stability. It is important to notice that cyber attacks are the biggest concern nowadays in smart grid stability studies. However, the proposed strategy can enhance the resiliency of the power system to any contingency that disrupts a communication channel of the central controller (which is not limited to cyber attacks but also includes other problems such as natural disasters).

Wide-area damping controller (WADC) uses remote signals to enhance the small-signal stability of large scale interconnected power systems. Many techniques have been proposed for the WADC design considering multiple operating points and time delay in the communication channels (Zhang et al. 2016). However, communication failures pose a challenge for wide-area damping controllers in power systems as shown in Khosravani et al. (2016), Padhy et al. (2017), Raoufat et al. (2017), Zhang and Vittal (2013) and Zhang and Vittal (2014). In Raoufat et al. (2017), Zhang and Vittal (2013) and Zhang and Vittal (2014), the authors propose to use redundant communication channels when a channel fails. However, this solution may increase the size of the controller and limit the number of signals that can be used in the controller. In Khosravani et al. (2016), the solution of the communication failure is the reconfiguration of the controller, but this requires the preservation of the system observability and the communication failure must be temporary. In Padhy et al. (2017), the resulting controller does not consider communication permanent failure, but it considers a specific group of packet dropout in the channels.

Based on the above, the main contributions of this paper are: to present a procedure based on linear matrix inequalities (LMIs) to design a WADC with robustness to multiple operating points and permanent communication channel losses due to DoS attacks or another event, which is different from the assumption made in the papers (Khosravani et al. 2016; Padhy et al. 2017; Raoufat et al. 2017; Zhang and Vittal 2013, 2014) discussed previously. The resulting controller will improve the damping of the closed-loop system even when a permanent communication channel loss occurs.

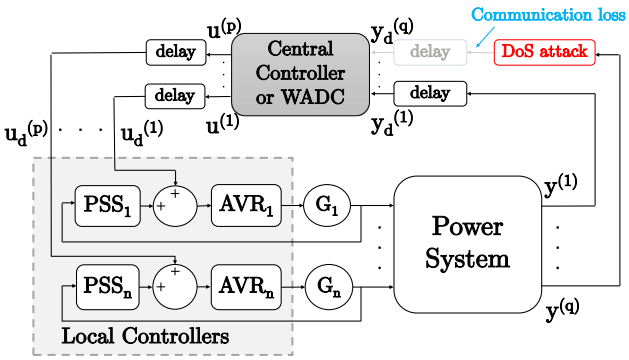

Fig. 1 Two-level control structure under DoS attack

The remaining of the paper is organized as follows. Section 2 presents the control structure used in this paper. Section 3 presents the power system modeling. The proposed robustness to signal loss is presented in Sect. 4. The design method based on LMI that considers robustness to communication signal losses is described in Sect. 5. In Sect. 6, the performance of the proposed method is evaluated through small-signal stability analysis and time-domain nonlinear simulations. Finally, concluding remarks are given in Sect. 7.

2 Control Structure

The control structure used in this paper is a two-level control scheme (Bento et al. 2017; Dotta et al. 2009) that comprises local controllers in a first level and a central controller in a second level. Figure 1 presents this scheme. The local controllers correspond to the conventional automatic voltage regulators (AVRs) with power system stabilizers (PSSs) at the generators (Gs). In this paper, the PSSs are assumed to be already installed and tuned at the generators and, so, the existing PSSs parameters settings will not be modified. The central controller design is the goal of this research, and its purpose is to improve the closed-loop system damping. The central controller is located in a central place with input and output signals transmitted from and to remote locations and, because of this, time delay must be considered, which is represented in Fig. 1 by the block *delay*. Usually, the PMU data are transmitted using the protocol of the IEEE C37.118 standard. This communication can be interrupted by DoS attacks jamming the communication channels, attacking network protocols or flooding the network traffic, and then, the measurement packets that are periodically used by the WADC can be lost. Figure 1 illustrates a communication loss of the first output of the power system. As a result, the

power system stability can be compromised if robustness of the WADC with respect to possible permanent communication loss was not treated in the design stage. The proposed procedure, which will be presented in this paper, will provide a single WADC that will improve the damping of the closed-loop system even when a permanent communication channel loss due to DoS attacks occurs in the input or in the output of the central controller.

3 System Model

3.1 Power System Model with the Local Controllers

The standard approach to power system modeling for damping controllers design is based on the linearization of the original state-space nonlinear power system model around a nominal operating point. For that, let us define $\mathbf{x} \in \mathbb{R}^n$ as being the state vector related to the state variables of the generators and the local controllers and, from Fig. 1, the vectors $\mathbf{u_d} = [u_d^{(1)} \ \cdots \ u_d^{(p)}]^{\mathrm{T}} \in \mathbb{R}^p$ and $\mathbf{y} = [y^{(1)} \ \cdots \ y^{(q)}]^{\mathrm{T}} \in \mathbb{R}^q$ as being, respectively, the input vector with the delayed output signals produced by the WADC and the output vector containing the speed signals of generators provided by PMUs. It is important to emphasize that other signals can be used as inputs for the WADC, such as voltages and angles measured from PMUs. These signals can be chosen from a residue analysis.

After the application of a standard linearization procedure around a nominal operating point, the power system model with the local controllers can be described by Kundur et al. (1994):

$$\dot{\mathbf{x}} = \mathbf{A}\mathbf{x} + \mathbf{B}\mathbf{u_d}, \tag{1}$$

$$\mathbf{y} = \mathbf{C}\mathbf{x} \tag{2}$$

where $\mathbf{A} \in \mathbb{R}^{n\times n}$, $\mathbf{B} \in \mathbb{R}^{n\times p}$ and $\mathbf{C} \in \mathbb{R}^{q\times n}$ are, respectively, the state, the input and output matrices of the power system model with the local controllers. Notice that, after the time delays in the input communication channels, the signals generated by the WADC are introduced to the AVRs of the generators.

3.2 Power System Model with the Local Controllers and Time Delays

Time delays in the communication channels are modeled in this paper by a second-order Padé approximation (De Campos and da Cruz 2016; Saraf et al. 2016). So, each block *delay* in Fig. 1 is given by the transfer function

$$\mathbf{G_d}(s) = \frac{T^2s^2 - 6Ts + 12}{T^2s^2 + 6Ts + 12} \tag{3}$$

where T is the time delay. A state-space realization can be obtained for each set of time delay models related to the input and output communication channels, in accordance with Fig. 1, and they are given by

$$\dot{\mathbf{x}}_{\mathbf{d_i}} = \mathbf{A}_{\mathbf{d_i}}\mathbf{x}_{\mathbf{d_i}} + \mathbf{B}_{\mathbf{d_i}}\mathbf{u} \tag{4}$$

$$\mathbf{u_d} = \mathbf{C}_{\mathbf{d_i}}\mathbf{x}_{\mathbf{d_i}} + \mathbf{D}_{\mathbf{d_i}}\mathbf{u} \tag{5}$$

where $\mathbf{x}_{\mathbf{d_i}}$ is the vector with the state variables of the input time delay models and $\mathbf{u} = [u^{(1)} \ \cdots \ u^{(p)}]^{\mathrm{T}} \in \mathbb{R}^p$ is the vector with the output signals of the WADC, as well as,

$$\dot{\mathbf{x}}_{\mathbf{d_o}} = \mathbf{A}_{\mathbf{d_o}}\mathbf{x}_{\mathbf{d_o}} + \mathbf{B}_{\mathbf{d_o}}\mathbf{y} \tag{6}$$

$$\mathbf{y_d} = \mathbf{C}_{\mathbf{d_o}}\mathbf{x}_{\mathbf{d_o}} + \mathbf{D}_{\mathbf{d_o}}\mathbf{y} \tag{7}$$

where $\mathbf{x}_{\mathbf{d_o}}$ is the vector with the state variables of the output time delay models and $\mathbf{y_d} = [y_d^{(1)} \ \cdots \ y_d^{(q)}]^{\mathrm{T}} \in \mathbb{R}^q$ is the vector with the delayed input signals for the WADC.

The time delays in the communication channels can be included in the power system model by incorporating (4)–(7) in Eqs. (1)–(2). Defining $\bar{\mathbf{x}} = \left[\mathbf{x} \ \mathbf{x}_{\mathbf{d_i}} \ \mathbf{x}_{\mathbf{d_o}}\right]^{\mathrm{T}}$, the power system model with the local controllers and time delays can be written in the state-space form as

$$\dot{\bar{\mathbf{x}}} = \bar{\mathbf{A}}\bar{\mathbf{x}} + \bar{\mathbf{B}}\mathbf{u} \tag{8}$$

$$\mathbf{y_d} = \bar{\mathbf{C}}\bar{\mathbf{x}} \tag{9}$$

where

$$\bar{\mathbf{A}} = \begin{bmatrix} \mathbf{A} & \mathbf{B}\mathbf{C}_{\mathbf{d_i}} & \mathbf{0} \\ \mathbf{0} & \mathbf{A}_{\mathbf{d_i}} & \mathbf{0} \\ \mathbf{B}_{\mathbf{d_o}}\mathbf{C} & \mathbf{0} & \mathbf{A}_{\mathbf{d_o}} \end{bmatrix}, \quad \bar{\mathbf{B}} = \begin{bmatrix} \mathbf{B}\mathbf{D}_{\mathbf{d_i}} \\ \mathbf{B}_{\mathbf{d_i}} \\ \mathbf{0} \end{bmatrix} \tag{10}$$

$$\bar{\mathbf{C}} = \begin{bmatrix} \mathbf{D}_{\mathbf{d_o}}\mathbf{C} \ \mathbf{0} \ \mathbf{C}_{\mathbf{d_o}} \end{bmatrix} \tag{11}$$

where $\bar{\mathbf{A}} \in \mathbb{R}^{r\times r}$, $\bar{\mathbf{B}} \in \mathbb{R}^{r\times p}$ and $\bar{\mathbf{C}} \in \mathbb{R}^{q\times r}$.

3.3 Central Controller

In this paper, the central controller (WADC) is based on dynamic output feedback control given in the state-space form by:

$$\dot{\mathbf{x}}_{\mathbf{c}} = \mathbf{A}_{\mathbf{c}}\mathbf{x}_{\mathbf{c}} + \mathbf{B}_{\mathbf{c}}\mathbf{y_d} \tag{12}$$

$$\mathbf{u} = \mathbf{C}_{\mathbf{c}}\mathbf{x}_{\mathbf{c}} \tag{13}$$

where $\mathbf{x_c}$ is the controller state vector, $\mathbf{A_c} \in \mathbb{R}^{m\times m}$, $\mathbf{B_c} \in \mathbb{R}^{m\times q}$ and $\mathbf{C_c} \in \mathbb{R}^{p\times m}$.

The central controller can be represented by a transfer function matrix, given by $\mathbf{CC}(s) = \mathbf{C_c}(s\mathbf{I} - \mathbf{A_c})^{-1}\mathbf{B_c}$ where

$$\mathbf{CC}(s) = \begin{bmatrix} cc_{11}(s) & \cdots & cc_{1q}(s) \\ \vdots & \ddots & \vdots \\ cc_{p1}(s) & \cdots & cc_{pq}(s) \end{bmatrix} \tag{14}$$

It is important to emphasize that the purpose of this paper is to design this central controller. The local controllers will be fixed and considered in power system model (1)–(2).

4 The Proposed Control Methodology for the WADC Design

4.1 Closed-Loop System

Using (8)–(9) to represent the power system with the local controllers and time delays in the input and output communication channels and including the WADC model given by (12)–(13), the closed-loop system can be represented by

$$\dot{\widetilde{\mathbf{x}}} = \widetilde{\mathbf{A}}\widetilde{\mathbf{x}} \tag{15}$$

where $\widetilde{\mathbf{x}} = \begin{bmatrix} \bar{\mathbf{x}} & \mathbf{x_c} \end{bmatrix}^{\mathrm{T}}$ and

$$\widetilde{\mathbf{A}} = \begin{bmatrix} \bar{\mathbf{A}} & \bar{\mathbf{B}}\mathbf{C_c} \\ \mathbf{B_c}\bar{\mathbf{C}} & \mathbf{A_c} \end{bmatrix} \tag{16}$$

The performance objective is to design a central controller for the closed-loop system (15), presenting a minimum damping (ζ_0) for all the eigenvalues of the state matrix $\widetilde{\mathbf{A}}$ greater than the safe margin of 5% (Gomes et al. 2003) for several operating conditions and even in the occurrence of communication permanent loss.

4.2 Robustness of the Central Controller with Respect to the Variations in the Operating Conditions

The robustness of the central controller with respect to the variations in the operating points of the system is dealt by obtaining a description of the power system model with the local controllers in the form of (1)–(2) with respect to several equilibrium points of interest, resulting in a set of linearized models in the form

$$\dot{\mathbf{x}}_j = \mathbf{A}_j\mathbf{x}_j + \mathbf{B}_j\mathbf{u}_{\mathbf{d}\,j}, \tag{17}$$

$$\mathbf{y}_j = \mathbf{C}_j\mathbf{x}_j \tag{18}$$

where $j = 1, \ldots, L$ represents the L operating points, $\mathbf{A}_j \in \mathbb{R}^{n\times n}$, $\mathbf{B}_j \in \mathbb{R}^{n\times p}$ and $\mathbf{C}_j \in \mathbb{R}^{q\times n}$. Also, $\mathbf{x}_j = \mathbf{x} - \mathbf{x}_{e_j}$, $\mathbf{u}_{\mathbf{d}\,j} = \mathbf{u}_{\mathbf{d}} - \mathbf{u}_{e_j}$ and $\mathbf{y}_j = \mathbf{y} - \mathbf{y}_{e_j}$, where $(\mathbf{x}_{e_j}, \mathbf{u}_{e_j})$ is the jth operating (or equilibrium) point of the system and $\mathbf{y}_{e_j}$ is the corresponding output operating point.

The purpose is to design a fixed parameter central controller in form (12)–(13) that exhibits an effective performance around all of these L points. The set of resulting closed-loop systems is described in state-space form by

$$\dot{\widetilde{\mathbf{x}}}_j = \widetilde{\mathbf{A}}_j\widetilde{\mathbf{x}}_j \tag{19}$$

where $\widetilde{\mathbf{x}}_j = \begin{bmatrix} \bar{\mathbf{x}}_j & \mathbf{x_c} \end{bmatrix}^{\mathrm{T}}$,

$$\widetilde{\mathbf{A}}_j = \begin{bmatrix} \bar{\mathbf{A}}_j & \bar{\mathbf{B}}_j\mathbf{C_c} \\ \mathbf{B_c}\bar{\mathbf{C}}_j & \mathbf{A_c} \end{bmatrix} \tag{20}$$

being $\bar{\mathbf{x}}_j = \begin{bmatrix} \mathbf{x}_j & \mathbf{x_{d_i}} & \mathbf{x_{d_o}} \end{bmatrix}^{\mathrm{T}}$, as well as,

$$\bar{\mathbf{A}}_j = \begin{bmatrix} \mathbf{A}_j & \mathbf{B}_j\mathbf{C_{d_i}} & \mathbf{0} \\ \mathbf{0} & \mathbf{A_{d_i}} & \mathbf{0} \\ \mathbf{B_{d_o}}\mathbf{C}_j & \mathbf{0} & \mathbf{A_{d_o}} \end{bmatrix}, \ \bar{\mathbf{B}} = \begin{bmatrix} \mathbf{B}_j\mathbf{D_{d_i}} \\ \mathbf{B_{d_i}} \\ \mathbf{0} \end{bmatrix} \tag{21}$$

$$\bar{\mathbf{C}} = \begin{bmatrix} \mathbf{D_{d_o}}\mathbf{C}_j & \mathbf{0} & \mathbf{C_{d_o}} \end{bmatrix} \tag{22}$$

and $j = 1, \ldots, L$.

4.3 Robustness of the Central Controller with Respect to Communication Permanent Loss

As discussed in the previous subsection, the desired performance criterion is given by a minimum damping value equal to 5% imposed to the eigenvalues of all closed-loop systems (20). Besides, the resulting controller must guarantee quadratic stability. This criterion must be satisfied when all the communication channels are active and also when communication channel losses occur at the input and at the output of the central controller.

For a centralized controller, the communication channel loss at the input or at the output can be interpreted as zeroing certain position of the matrices $\bar{\mathbf{B}}$ and $\bar{\mathbf{C}}$ related to the lost channel. In this paper, it is considered the loss of only one communication channel at a time, or at the input or at the output of the central controller.

Then, considering the central controller with q inputs and p output channels, if the loss of communication channel occurs at the input s ($s \in \mathbb{N}$, $1 \leq s \leq q$) of the central controller (that is, the sth generator speed signal is lost), the sth row of the matrix $\bar{\mathbf{C}} \in \mathbb{R}^{q\times r}$ must be zeroed, leading to the matrix $\bar{\mathbf{C}}^s$. If the loss of communication channel occurs at the output t ($t \in \mathbb{N}$, $1 \leq t \leq p$) of the central controller (that is, the tth stabilizing signal produced by the WADC is lost), the tth column of the matrix $\bar{\mathbf{B}} \in \mathbb{R}^{r\times p}$ must be zeroed, leading to the matrix $\bar{\mathbf{B}}^t$.

This procedure of zeroing the rows and columns does not affect the original dimensions of the matrices $\bar{\mathbf{B}}$ and $\bar{\mathbf{C}}$, and then, the sets $\mathbf{F}_{\bar{\mathbf{B}}_j} = \bar{\mathbf{B}}_j \cup \{\bar{\mathbf{B}}_j^t : t = 1, \ldots, p\}$ and $\mathbf{F}_{\bar{\mathbf{C}}_j} = \bar{\mathbf{C}}_j \cup \{\bar{\mathbf{C}}_j^s : s = 1, \ldots, q\}$ can be considered, where $\bar{\mathbf{B}}_j$ and $\bar{\mathbf{C}}_j$ are the input and output matrices, respectively, for the case where all the communication channels are actives and $j = 1, \ldots, L$.

Thus, it is possible to define a set of closed-loop system matrices for the jth operating condition as

$$\mathbf{F}_{\breve{\mathbf{A}}j} = \left\{ \begin{bmatrix} \bar{\mathbf{A}}_j & \breve{\mathbf{B}}_j\mathbf{C_c} \\ \mathbf{B_c}\bar{\mathbf{C}}_j & \mathbf{A_c} \end{bmatrix} : \breve{\mathbf{B}}_j \in \mathbf{F}_{\bar{\mathbf{B}}_j} \right\} \cup \left\{ \begin{bmatrix} \bar{\mathbf{A}}_j & \bar{\mathbf{B}}_j\mathbf{C_c} \\ \mathbf{B_c}\breve{\mathbf{C}}_j & \mathbf{A_c} \end{bmatrix} : \breve{\mathbf{C}}_j \in \mathbf{F}_{\bar{\mathbf{C}}_j} \right\}$$

where $j = 1, \ldots, L$. The robustness of the central controller with respect to the variations in the operating conditions and communication permanent loss is guaranteed by finding a matrix $\mathbf{P} = \mathbf{P}^{\mathrm{T}} \succ 0$ of proper dimension, as well as, the central controller matrices $\mathbf{A_c}$, $\mathbf{B_c}$ and $\mathbf{C_c}$ such that

$$\breve{\mathbf{A}}_j^{\mathrm{T}}\mathbf{P} + \mathbf{P}\breve{\mathbf{A}}_j \prec 0 \tag{23}$$

for all $\breve{\mathbf{A}}_j \in \mathbf{F}_{\breve{\mathbf{A}}j}$ and $j = 1, \ldots, L$.

In order to guarantee not only stability to the closed-loop systems, but also a minimum damping (ζ_0) for all the eigenvalues of all matrices in the sets $\mathbf{F}_{\mathbf{A}j}$, $j = 1, \ldots, L$, the problem can be formulated by finding a matrix $\mathbf{P} = \mathbf{P}^{\mathrm{T}} \succ 0$ of proper dimension, as well as, the central controller matrices $\mathbf{A_c}$, $\mathbf{B_c}$ and $\mathbf{C_c}$, such that

$$\begin{bmatrix} \sin(\theta)(\breve{\mathbf{A}}_j^{\mathrm{T}}\mathbf{P} + \mathbf{P}\breve{\mathbf{A}}_j) & \cos(\theta)(\breve{\mathbf{A}}_j^{\mathrm{T}}\mathbf{P} - \mathbf{P}\breve{\mathbf{A}}_j) \\ \cos(\theta)(\breve{\mathbf{A}}_j^{\mathrm{T}}\mathbf{P} - \mathbf{P}\breve{\mathbf{A}}_j)^{\mathrm{T}} & \sin(\theta)(\breve{\mathbf{A}}_j^{\mathrm{T}}\mathbf{P} + \mathbf{P}\breve{\mathbf{A}}_j) \end{bmatrix} \prec 0 \tag{24}$$

for all $\breve{\mathbf{A}}_j \in \mathbf{F}_{\breve{\mathbf{A}}j}$ and $j = 1, \ldots, L$, where $\theta = \arccos(\zeta_0)$.

Matrix inequalities (24) are nonlinear in the variables $\mathbf{P}$, $\mathbf{A_c}$, $\mathbf{B_c}$ and $\mathbf{C_c}$. In order to transform this inequalities to linear matrix inequalities (LMIs), this paper adopts the parametrization proposed in Ramos et al. (2004). The next section presents the proposed procedure design based on the solution of a set of LMIs.

5 Proposed Design Procedure Based on LMIs

Step 1: Choose L operating points and linearize the system equations around these points obtaining $\mathbf{A}_j$, $\mathbf{B}_j$ and $\mathbf{C}_j$. Include the time delay model obtaining $\bar{\mathbf{A}}_j$, $\bar{\mathbf{B}}_j$ and $\bar{\mathbf{C}}_j$.
Step 2: Build the matrices that will consider the communication permanent loss and construct the sets $\mathbf{F}_{\bar{\mathbf{B}}_j}$ and $\mathbf{F}_{\bar{\mathbf{C}}_j}$, $j = 1, \ldots, L$.
Step 3: Define the minimum damping ratio ζ_0 required and calculate $\theta = \arccos(\zeta_0)$.
Step 4: Build the computational representation of the matrix variables $\mathbf{Y}$ and $\mathbf{L}$ and of the LMIs

$$\mathbf{Y} \succ \mathbf{0} \tag{25}$$

$$\begin{bmatrix} \mathbf{N}_{11} & \mathbf{N}_{12} \\ \mathbf{N}_{12}^{\mathrm{T}} & \mathbf{N}_{22} \end{bmatrix} \prec \mathbf{0} \tag{26}$$

where

$$\mathbf{N}_{11} = \mathbf{N}_{22} = \sin(\theta)(\bar{\mathbf{A}}_j\mathbf{Y} + \mathbf{Y}\bar{\mathbf{A}}_j^{\mathrm{T}} + \breve{\mathbf{B}}\mathbf{L} + \mathbf{L}^{\mathrm{T}}\breve{\mathbf{B}}^{\mathrm{T}}) \tag{27}$$

$$\mathbf{N}_{12} = \cos(\theta)(\mathbf{Y}\bar{\mathbf{A}}_j^{\mathrm{T}} - \bar{\mathbf{A}}_j\mathbf{Y} + \mathbf{L}^{\mathrm{T}}\breve{\mathbf{B}}^{\mathrm{T}} - \breve{\mathbf{B}}\mathbf{L}) \tag{28}$$

for $\breve{\mathbf{B}}_j \in \mathbf{F}_{\bar{\mathbf{B}}_j}$, $j = 1, \ldots, L$.
Step 5: Apply an LMI solver on (25) and (26) to find $\mathbf{Y}$ and $\mathbf{L}$ and, then, calculate $\mathbf{C_c} = \mathbf{L}\mathbf{Y}^{-1}$.
Step 6: Define the sets $\mathbf{F}_{\widehat{\mathbf{A}}j} = \{\bar{\mathbf{A}} + \breve{\mathbf{B}}\mathbf{C_c} : \breve{\mathbf{B}} \in \mathbf{F}_{\bar{\mathbf{B}}_j}\}$, $j = 1, \ldots, L$.
Step 7: Build the computational representation of matrix variables $\mathbf{P}$, $\mathbf{X}$, $\mathbf{W}$ and $\mathbf{S}$ and of the LMIs

$$\begin{bmatrix} \mathbf{P} & \mathbf{P} \\ \mathbf{P} & \mathbf{X} \end{bmatrix} \succ \mathbf{0} \tag{29}$$

$$\begin{bmatrix} \mathbf{M}_{11} & \mathbf{M}_{12} & \mathbf{M}_{13} & \mathbf{M}_{14} \\ \mathbf{M}_{12}^{\mathrm{T}} & \mathbf{M}_{22} & \mathbf{M}_{23} & \mathbf{M}_{24} \\ \mathbf{M}_{13}^{\mathrm{T}} & \mathbf{M}_{23}^{\mathrm{T}} & \mathbf{M}_{33} & \mathbf{M}_{34} \\ \mathbf{M}_{14}^{\mathrm{T}} & \mathbf{M}_{24}^{\mathrm{T}} & \mathbf{M}_{34}^{\mathrm{T}} & \mathbf{M}_{44} \end{bmatrix} \prec \mathbf{0} \tag{30}$$

where

$$\mathbf{M}_{11} = \sin(\theta)(\mathbf{P}\widehat{\mathbf{A}}_j + \widehat{\mathbf{A}}_j^{\mathrm{T}}\mathbf{P})$$
$$\mathbf{M}_{12} = \sin(\theta)(\mathbf{P}\bar{\mathbf{A}}_j + \widehat{\mathbf{A}}_j^{\mathrm{T}}\mathbf{X} + \breve{\mathbf{C}}_j^{\mathrm{T}}\mathbf{W}^{\mathrm{T}} + \mathbf{S})$$
$$\mathbf{M}_{13} = \cos(\theta)(\widehat{\mathbf{A}}_j^{\mathrm{T}}\mathbf{P} - \mathbf{P}\widehat{\mathbf{A}}_j^{\mathrm{T}})$$
$$\mathbf{M}_{14} = \cos(\theta)(-\mathbf{P}\bar{\mathbf{A}}_j + \widehat{\mathbf{A}}_j^{\mathrm{T}}\mathbf{X} + \breve{\mathbf{C}}_j^{\mathrm{T}}\mathbf{W}^{\mathrm{T}} + \mathbf{S})$$
$$\mathbf{M}_{22} = \sin(\theta)(\mathbf{X}\bar{\mathbf{A}}_j + \bar{\mathbf{A}}_j^{\mathrm{T}}\mathbf{X} + \mathbf{W}\breve{\mathbf{C}}_j + \breve{\mathbf{C}}_j^{\mathrm{T}}\mathbf{W}^{\mathrm{T}})$$
$$\mathbf{M}_{23} = \mathbf{M}_{14}^{\mathrm{T}}$$
$$\mathbf{M}_{24} = \cos(\theta)(-\mathbf{X}\bar{\mathbf{A}}_j + \bar{\mathbf{A}}_i^{\mathrm{T}}\mathbf{X} - \mathbf{W}\breve{\mathbf{C}}_j + \breve{\mathbf{C}}_j^{\mathrm{T}}\mathbf{W}^{\mathrm{T}})$$
$$\mathbf{M}_{33} = \mathbf{M}_{11}$$
$$\mathbf{M}_{34} = \mathbf{M}_{12}$$
$$\mathbf{M}_{44} = \mathbf{M}_{22}$$

for all $\widehat{\mathbf{A}}_j \in \mathbf{F}_{\widehat{\mathbf{A}}j}$, $\breve{\mathbf{C}}_j \in \mathbf{F}_{\bar{\mathbf{C}}_j}$, $j = 1, \ldots, L$.
Step 7: Apply an LMI solver on (29) and (30) to find $\mathbf{P}$, $\mathbf{X}$, $\mathbf{W}$ and $\mathbf{S}$.
Step 8: Calculate $\mathbf{U} = \mathbf{P} - \mathbf{X}$ and $\mathbf{B_c} = \mathbf{U}^{-1}\mathbf{W}$.

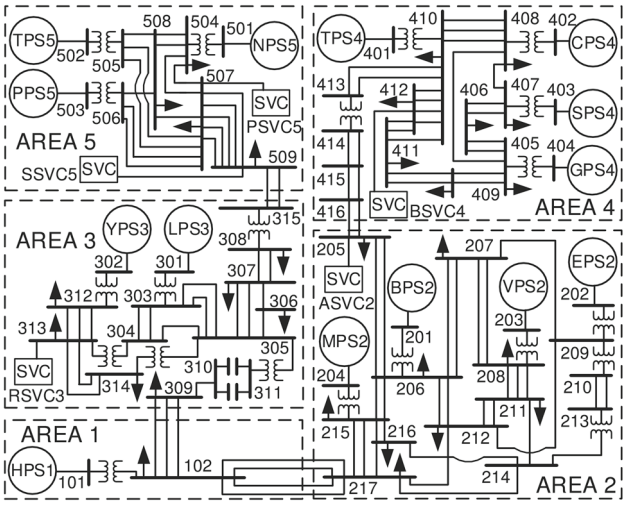

Fig. 2 IEEE simplified 14-generator Australian power system (Canizares et al. 2017)

Step 9: Calculate $\mathbf{Z} = \mathbf{P}^{-1}\mathbf{S}$ and $\mathbf{A_c} = \mathbf{U}^{-1}\mathbf{Z}^{\mathrm{T}}\mathbf{P}$.

In this work, it was used the SeDuMi solver (Sturm 1999) for the proposed procedure and the balanced truncation for the controller reduction (Safonov and Chiang 1989).

6 Numerical Results

The performance of the proposed method is assessed through its application to the Simplified 14-Generator Model of the Southeastern Australian Power System (Canizares et al. 2017), shown in Fig. 2. This system is one of the IEEE standard benchmark models for the analysis and control of small-signal oscillatory dynamics in power systems. This system presents 14 generators of fifth and sixth order, 5 static VAR compensators (SVCs), 59 buses and 104 lines with voltage levels ranging from 15 to 500 kV and 6 operating cases presented in Canizares et al. (2017). Three IEEE standard types of excitation systems are employed: ST5B, AC4A and AC1A. The order of the state-space model is 174. The system has been divided into 5 areas, and there are 3 inter-area modes and 10 local-area modes for the 6 operating cases. Without PSSs, most of the electromechanical models are unstable. Because of this, 14 PSSs were designed, one for each generator, and the minimum damping for the 6 operating cases is higher than 15%. The designed PSSs are shown in Canizares et al. (2017).

However, if the transmission lines 207–209 and 209–212 are inactive for the 6 operating cases (contingency C1), or similarly, lines 214–216 and 214–217 (contingency C2), there exists an oscillation mode poorly damped, or even unstable, as it can be seen in Table 1 and Fig. 3. This table shows the dominant oscillation mode (that is, the oscillation mode with the lowest damping ratio) for each contingency

Table 1 System dominant oscillation modes without WADC

Case	Eigenvalue	Freq. (Hz)	Damp. (%)
C1 (The worst of 6)	$0.19 \pm 7.72i$	1.23	−2.44
C2 (The worst of 6)	$-0.26 \pm 7.83i$	1.25	3.35

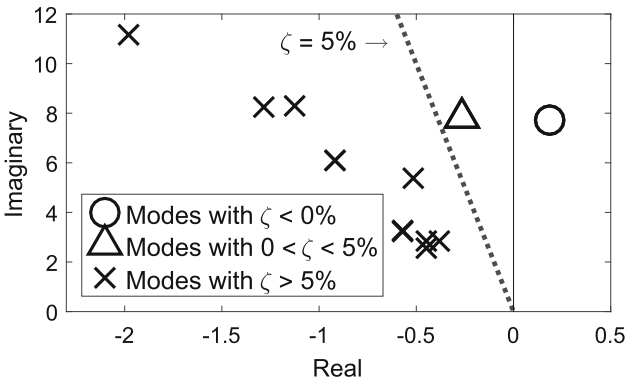

Fig. 3 Dominant eigenvalues of each operating condition

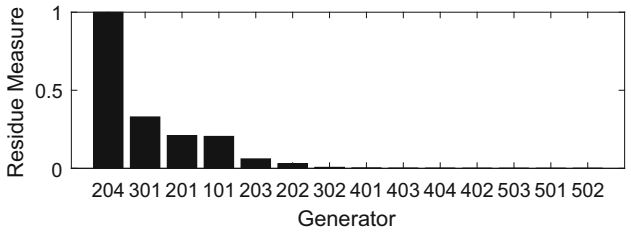

Fig. 4 Residue measure of the mode 1 (C1)

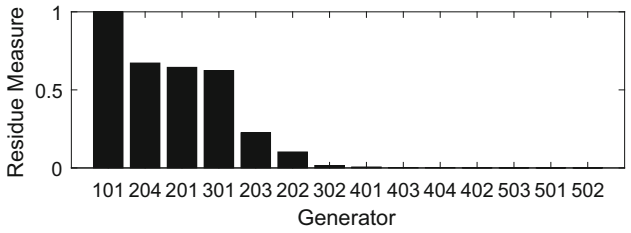

Fig. 5 Residue measure of the mode 2 (C2)

(C1 and C2) among the 6 operating cases, where only the worst case is shown. As it can be seen, the designed PSSs did not provide a good performance for these contingencies in analysis. In order to improve the system damping when it is exposed to these contingencies, a centralized controller (WADC) is required to design.

Table 2 System dominant oscillation modes with two-level control and robustness to communication signal loss

Case	Eigenvalue	Freq. (Hz)	Damping (%)
All 108	$-0.10 \pm 2.03i$	0.32	5.01

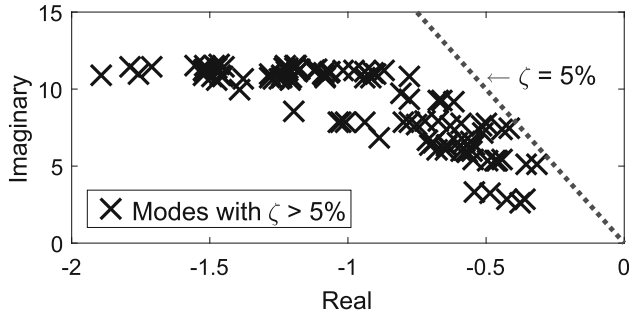

Fig. 6 Dominant eigenvalues of each one of the 108 scenarios

Table 3 System dominant oscillation modes with two-level control

Case	Signal loss	Eigenvalue	Freq. (Hz)	Damp. (%)
C1	None	$-0.6161 \pm 9.2132i$	1.4663	6.6724
	$\Delta\omega_{101}$	$-0.4157 \pm 7.4523i$	1.1861	5.5696
	$\Delta\omega_{201}$	$-0.6620 \pm 9.2900i$	1.4785	7.1075
	$\Delta\omega_{204}$	$-0.6724 \pm 9.2289i$	1.4688	7.2664
	$\Delta\omega_{301}$	$-0.3139 \pm 5.1120i$	0.8136	6.1293
	$V_{\text{REF\_101}}$	$-0.3535 \pm 5.1506i$	0.8198	6.8474
	$V_{\text{REF\_201}}$	$-0.4417 \pm 7.4128i$	1.1798	5.9478
	$V_{\text{REF\_204}}$	$-0.5127 \pm 7.1119i$	1.1319	7.1902
	$V_{\text{REF\_301}}$	$-0.7756 \pm 9.3563i$	1.4891	8.2616
C2	None	$-0.6407 \pm 6.3203i$	1.0059	10.0858
	$\Delta\omega_{101}$	$-0.6728 \pm 7.9656i$	1.2678	8.4161
	$\Delta\omega_{201}$	$-0.8074 \pm 9.7046i$	1.5445	8.2916
	$\Delta\omega_{204}$	$-0.5436 \pm 6.3485i$	1.0104	8.5311
	$\Delta\omega_{301}$	$-0.6922 \pm 6.4910i$	1.0331	10.6043
	$V_{\text{REF\_101}}$	$-0.7047 \pm 6.3452i$	1.0099	11.0375
	$V_{\text{REF\_201}}$	$-0.5535 \pm 6.5761i$	1.0466	8.3868
	$V_{\text{REF\_204}}$	$-0.7507 \pm 7.6573i$	1.2187	9.7567
	$V_{\text{REF\_301}}$	$-0.6435 \pm 6.3290i$	1.0073	10.1157

Thus, the first step is to design a central controller that ensures the closed-loop system with minimum damping higher than 5%. In addition, the same central controller must be robust to possible communication signal losses in the input and output of the controller.

6.1 Choice of Central Controller Input and Output Signals

The residue method based on modal analysis (Kundur et al. 1994) was used to choose the input and output signals of the central controller. For the application of this method, the generator speed signal $\Delta\omega$ as output of the system and the reference voltage signal V_{REF} applied to the AVR as input of the system were chosen. Figures 4 and 5 show the residue measure of the modes of Table 1. Based on the results, the generators 101, 201, 204 and 301 present the highest residue values. Thus, these four generator signals were chosen as input and output of the central controller design.

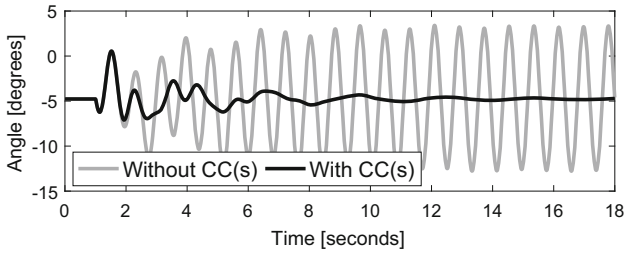

Fig. 7 Angle of the generator 101 for C1 and a temporary three-phase short circuit

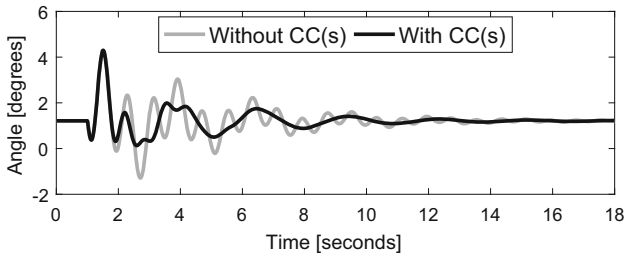

Fig. 8 Angle of the generator 101 for C2 and a temporary three-phase short circuit

The test system has 6 operating cases, and considering the two contingencies of Table 1, there are 12 operating conditions for the control design. However, we must consider robustness to communication permanent loss. Four signals for the central controller were defined, and considering as allowed one communication permanent loss, there are 9 possibilities of operation of the central controller: no signal loss, four generator speed signal losses ($\Delta\omega_{101}$, $\Delta\omega_{201}$, $\Delta\omega_{204} and \Delta\omega_{301}$) and four control signal losses ($V_{\text{REF\_101}}$, $V_{\text{REF\_201}}$, $V_{\text{REF\_204}}$ and $V_{\text{REF\_301}}$). So the central control design must consider the 108 scenarios (12 operating cases $\times$ 9 ways of operation of the central controller) of this closed-loop system.

6.2 Application of the Method Based on LMIs Considering Robustness to Communication Permanent Loss

Defining the minimum damping in $\zeta_0 = 5\%$, the operating point number in $L = 12$, time delays of 200 ms and applying the algorithm based on LMI of Sect. 5 in a computer with Intel Xeon of 2.40 GHz and 64 GB of RAM, the convergence of the procedure took 14 h.

The resulting controller is presenting in (31), and Table 2 shows the dominant oscillation modes with two-level control when there is no signal loss and there is a single loss of signal

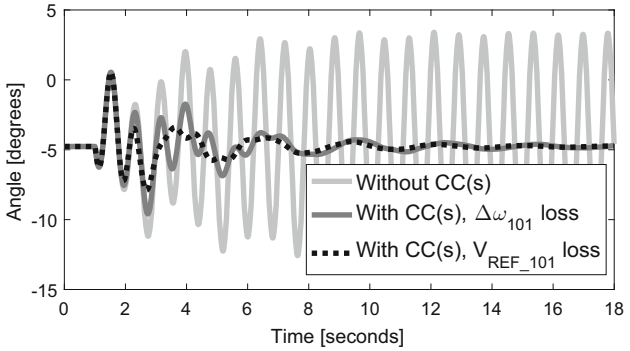

(a) $\Delta\omega_{101}$ signal loss and V_{REF_101} signal loss at a time.

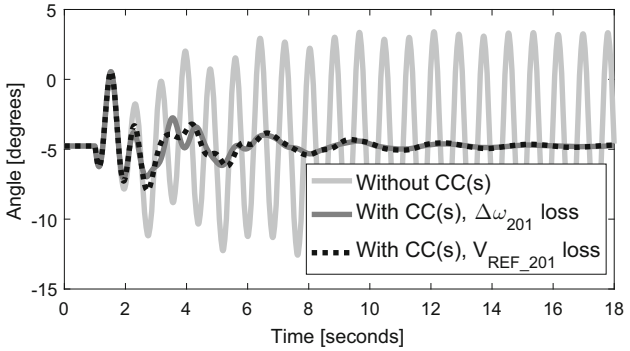

(b) $\Delta\omega_{201}$ signal loss and V_{REF_201} signal loss at a time.

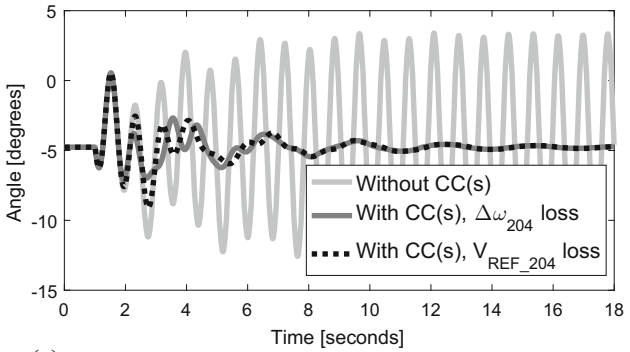

(c) $\Delta\omega_{204}$ signal loss and V_{REF_204} signal loss at a time.

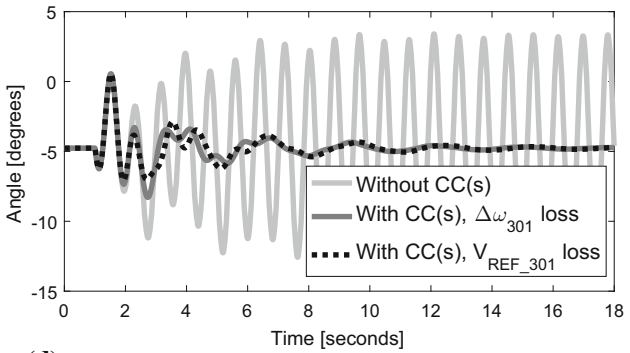

(d) $\Delta\omega_{204}$ signal loss and V_{REF_204} signal loss at a time.

Fig. 9 Angle of the generator 101 for C1 with and without **CC**(s) and one signal loss at a time

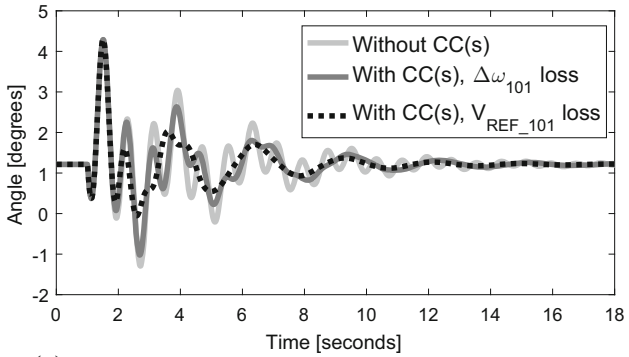

(a) $\Delta\omega_{101}$ signal loss and V_{REF_101} signal loss at a time.

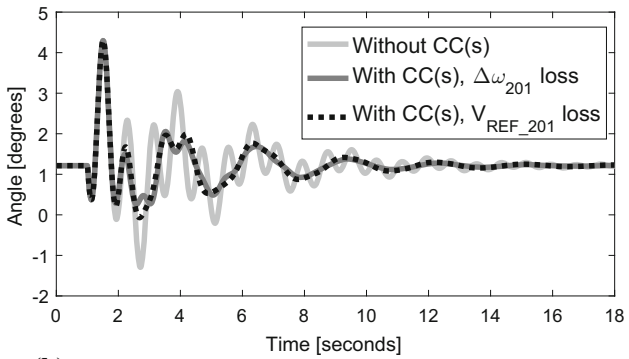

(b) $\Delta\omega_{201}$ signal loss and V_{REF_201} signal loss at a time.

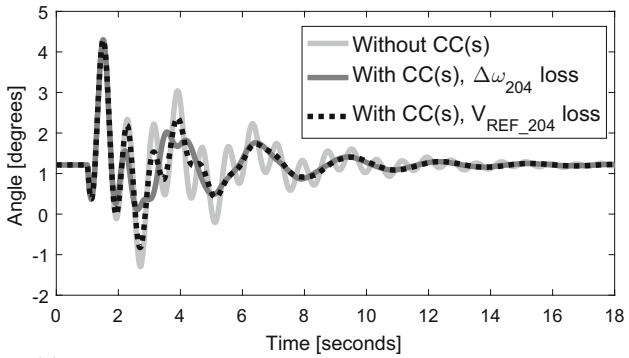

(c) $\Delta\omega_{204}$ signal loss and V_{REF_204} signal loss at a time.

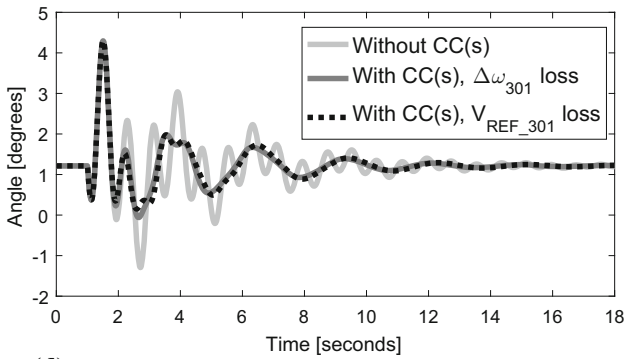

(d) $\Delta\omega_{301}$ signal loss and V_{REF_301} signal loss at a time.

Fig. 10 Angle of the generator 101 for C2 with and without **CC**(s) and one signal loss at a time

of the central controller for all 108 scenarios. As can be seen, all modes present damping higher than 5%.

Figure 6 presents the modes with minimum damping of each one of the 108 scenarios of the test system with two-level control. As you can see, all modes present damping higher than 5%.

Table 3 provides the dominant oscillation modes for the two operating points C1 and C2 of Table 1 for the system with two-level control when there is and there is no loss of channel for the controller. As can be seen, all scenarios present a damping higher than 5%.

Based on the results of modal analysis and time-domain nonlinear simulations, the central controller designed by the proposed algorithm provided good damping to the system even when a single remote communication link is lost. Among the perspective of future work is the extension of this guarantee to situations where the loss of more than one communication link occurs.

The main drawback related to methods based on LMIs is the presence of Lyapunov variables, whose dimensions grow quadratically with the system size. As a result, current LMI solvers quickly break down when plants get sizeable. So, a future work also is to evaluate the performance of the proposed procedure for power system models larger than the IEEE Australian Equivalent Model used in this paper and with wind generation.

$$\mathbf{CC}(s) = \begin{bmatrix} \frac{57.6s^2-239.3s+7973.5}{s^3+107s^2+1911s+9388} & \frac{5260.5s^2-31466s+78.3}{s^3+107s^2+1911s+9388} & \frac{1640.8s^2-270.3s-1593.8}{s^3+107s^2+1911s+9388} & \frac{-30861s^2-9308.8s-5924}{s^3+107s^2+1911s+9388} \\ \frac{196.8s^2+5074.3s-3977.3}{s^3+107s^2+1911s+9388} & \frac{-253.8s^2-82.5s+4278.9}{s^3+107s^2+1911s+9388} & \frac{-281.8s^2+131s-6258.1}{s^3+107s^2+1911s+9388} & \frac{-206.2s^2-14013s+9139}{s^3+107s^2+1911s+9388} \\ \frac{-193.9s^2+12814s+2741.7}{s^3+107s^2+1911s+9388} & \frac{-180.5s^2-4902.1s+8504}{s^3+107s^2+1911s+9388} & \frac{-164.1s^2-2534.5s-304.2}{s^3+107s^2+1911s+9388} & \frac{66.7s^2-6652.9s-211.6}{s^3+107s^2+1911s+9388} \\ \frac{183.6s^2+241.5s-8729.9}{s^3+107s^2+1911s+9388} & \frac{-208s^2+97.8s-57.7}{s^3+107s^2+1911s+9388} & \frac{296.3s^2-63.9s+4414.8}{s^3+107s^2+1911s+9388} & \frac{2119s^2-180.6s+11823}{s^3+107s^2+1911s+9388} \end{bmatrix} \quad (31)$$

6.3 Time-Domain Nonlinear Simulations

The performance of the central controller was evaluated by time-domain nonlinear simulations using ANATEM software (CEPEL 2014) in order to verify the design effectiveness of the nonlinear system. Limits of the AVR-PSS and the central controller were considered. The output limits of the AVRs and PSSs are the same presented in the benchmark and can be found in Canizares et al. (2017). The WADC limits chosen were the same for the output signals of the PSS $(-0.1, +0.1)$. A 15 ms three-phase short circuit was applied at bus 101 and cleared without any switching. The angle of the generator 101 for the contingencies C1 and C2 is presented in Figs. 7, 8, 9 and 10 considering no signal loss and one signal loss at a time. As you can see, the angular responses with the robust central controller are better damped than the response without the controller.

7 Conclusions

This paper presented a procedure based on LMIs to design a central controller with robustness to multiple operating points and communication channel failure caused, for example, by DoS attacks, a major concern nowadays in smart grid stability. Besides, a pre-specified minimum damping is incorporated in the LMI formulation in order to improve the closed-loop system damping. Time delays are also incorporated in the modeling.

References

Bento, M. E. C., Dotta, D., & Ramos, R. A. (2017). Wide-area measurements-based two-level control design considering power system operation uncertainties. In *2017 IEEE Manchester PowerTech*, IEEE (pp. 1–6).

Biswal, M., Brahma, S. M., & Cao, H. (2016). Supervisory Protection and automated event diagnosis using PMU data. *IEEE Transactions on Power Delivery*, *31*(4), 1855–1863.

Canizares, C., Fernandes, T., Geraldi, E., Gerin-Lajoie, L., et al. (2017). Benchmark models for the analysis and control of small-signal oscillatory dynamics in power systems. *IEEE Transactions on Power Systems*, *32*(1), 715–722.

CEPEL. (2014). Anatem user's manual version 10.5.2. Available: http://www.dre.cepel.br/.

De Campos, V. A. F., & da Cruz, J. J. (2016). Robust hierarchized controllers using wide area measurements in power systems. *International Journal of Electrical Power and Energy Systems*, *83*, 392–401.

De La Ree, J., Centeno, V., Thorp, J. S., & Phadke, A. G. (2010). Synchronized phasor measurement applications in power systems. *IEEE Transactions on Smart Grid*, *1*(1), 20–27.

Dotta, D., e Silva, A. S., & Decker, I. C. (2009). Wide-area measurements-based two-level control design considering signal transmission delay. *IEEE Transactions on Power Systems*, *24*(1), 208–216.

Farraj, A., Hammad, E., & Kundur, D. (2018). A cyber-physical control framework for transient stability in smart grids. *IEEE Transactions on Smart Grid*, *9*(2), 1205–1215.

Ghahremani, E., & Kamwa, I. (2016). Local and wide-area PMU-based decentralized dynamic state estimation in multi-machine power systems. *IEEE Transactions on Power Systems*, *31*(1), 547–562.

Ghorbani, A., Ghorbani, M., & Ebrahimi, S. Y. (2017). Synchrophasors-based transmission line protection in the presence of STATCOM. *Journal of Control, Automation and Electrical Systems*, *28*(1), 147–157.

Gomes, S., Martins, N., & Portela, C. (2003). Computing small-signal stability boundaries for large-scale power systems. *IEEE Transactions on Power Systems*, *18*(2), 747–752.

Khosravani, S., Naziri Moghaddam, I., Afshar, A., & Karrari, M. (2016). Wide-area measurement-based fault tolerant control of power system during sensor failure. *Electric Power Systems Research*, *137*, 66–75.

Kundur, P., Balu, N. J., & Lauby, M. G. (1994). *Power system stability and control* (Vol. 7). New York: McGraw-Hill.

Li, F., Qiao, W., Sun, H., Wan, H., Wang, J., Xia, Y., et al. (2010). Smart transmission grid: Vision and framework. *The IEEE Transactions on Smart Grid*, *1*(2), 168–177.

Liu, S., Liu, X. P., & El Saddik, A. (2013), Denial-of-service (dos) attacks on load frequency control in smart grids. In *2013 IEEE PES innovative smart grid technologies conference (ISGT), IEEE* (pp. 1–6).

Padhy, B. P., Srivastava, S. C., & Verma, N. K. (2017). A wide-area damping controller considering network input and output delays and packet drop. *IEEE Transactions on Power Systems*, *32*(1), 166–176.

Ramos, R. A., Alberto, L. F. C., & Bretas, N. G. (2004). A new methodology for the coordinated design of robust decentralized power system damping controllers. *IEEE Transactions on Power Systems*, *19*(1), 444–454.

Raoufat, M. E., Tomsovic, K., & Djouadi, S. M. (2017). Dynamic control allocation for damping of inter-area oscillations. *IEEE Transactions on Power Systems*, *32*(6), 4894–4903.

Safonov, M. G., & Chiang, R. Y. (1989). A Schur method for balanced-truncation model reduction. *IEEE Transactions on Automatic Control*, *34*(7), 729–733.

Saraf, P., Balasubramaniam, K., Hadidi, R., & Makram, E. (2016). Design of a wide area damping controller based on partial right eigenstructure assignment. *Electric Power Systems Research*, *134*, 134–144.

Sikdar, B., & Chow, J. H. (2011). Defending synchrophasor data networks against traffic analysis attacks. *IEEE Transactions on Smart Grid*, *2*(4), 819–826.

Sturm, J. F. (1999). Using SeDuMi 1.02: A Matlab toolbox for optimization over symmetric cones. *Optimization Methods and Software*, *11*(1–4), 625–653.

Surinkaew, T., & Ngamroo, I. (2016). Hierarchical co-ordinated wide area and local controls of DFIG wind turbine and PSS for robust power oscillation damping. *The IEEE Transactions on Sustainable Energy*, *7*(3), 943–955.

Tran, V. K., & Zhang, H. S. (2018). Optimal PMU placement using modified greedy algorithm. *Journal of Control, Automation and Electrical Systems*, *29*(1), 99–109.

Zhang, S., & Vittal, V. (2013). Design of wide-area power system damping controllers resilient to communication failures. *IEEE Transactions on Power Systems*, *28*(4), 4292–4300.

Zhang, S., & Vittal, V. (2014). Wide-area control resiliency using redundant communication paths. *IEEE Transactions on Power Systems*, *29*(5), 2189–2199.

Zhang, X., Lu, C., Liu, S., & Wang, X. (2016). A review on wide-area damping control to restrain inter-area low frequency oscillation for large-scale power systems with increasing renewable generation. *Renewable and Sustainable Energy Reviews*, *57*, 45–58.

Zhao, J., Zhang, G., Das, K., Korres, G. N., et al. (2016). Power system real-time monitoring by using PMU-based robust state estimation method. *IEEE Transactions on Smart Grid*, *7*(1), 300–309.